

Constant Flux Particle-laden Viscous Thin Film Flows on an Incline

Patrick Flynn^a, Joseph Pappe^b, Aviva Prins^{b,c},
William Sisson^d, Samuel Stanton^e, Ruiyi Yang^b

^a*California State University, Long Beach*

^b*University of California, Los Angeles*

^c*Santa Monica College*

^d*Lipscomb University*

^e*University of Colorado, Denver*

August 12, 2016

Abstract

We study the behaviour of particle-laden thin-films down an incline. Previous research focused on the finite volume case, whereas we consider the constant flow case with the aid of a pump. We model the problem as a Riemann problem. Experiments are done to obtain height profiles, front positions, surface velocities and observe different regimes. The model gives qualitative predictions of the separation of regimes and the linear dependence on time of the front positions. One important observation is that the timescales for the regimes to occur are longer than the finite volume case.

1 Introduction

During 2011-2015, the UCLA particle slurry group summer REUs investigated the behavior of thin film gravity-driven flow on an incline surface. The fluid was viscous, particle-laden, and constant volume. This basic research has applications such as mud slides, oil spills, spiral separators, food industry, and industrial painting.

On this topic, there was a surprising gap in the fluid dynamics literature. Through physical experimentation, model creation, and numerical simulation, these REUs identified and explained many of this scenario's unique phenomena, helping to fill the literature gap.

Particles were added to a viscous fluid to create an initial slurry of uniform particle concentration. This was found to change the behavior of the thin film flow, the type and degree of change depending on the experimental parameters: incline angle, fluid viscosity, and particle density. The measurements and observations taken at various times were fluid height profile, particle behavior, and fluid/particle front speeds and locations. Particle behavior was classified into three states. Well-mixed is the initial uniform particle concentration state. If the experimental incline surface is long enough, this state ultimately transitions to either the settled or ridged state. In the settled state, the particles, no longer suspended in the fluid, flow down directly on the inclined substrate. In the ridge state, the particles have trended towards the top of the fluid front, forming there a more particle dense suspension with an elevated height profile.

The particle slurry project of the first UCLA Applied Math REU in 2011 [1] used positively and neutrally buoyant particles to experimentally confirm the models and/or experiments of Huppert [2], Cook [3], and Ward [4]. The ridge front location was found to roughly follow Huppert's $x = Ct^{1/3}$ scaling.

The 2012 REU [5] focused on the flow of bidisperse suspensions of negatively buoyant lighter glass and heavier ceramic beads. If the two types of beads separated, the ceramic beads migrated above the glass beads and the glass beads tended to travel faster down the incline. When the incline angle, particle concentrations, and fluid viscosity led to a glass bead ridge effect, increasing the ceramic bead concentration would eventually cause an overall settled state.

The 2013-14 REUs [6] [7] investigated more deeply the effect of the experimental parameters on both mono- and bidisperse fluid flows. An attempt was made to experimentally determine a value for the C coefficient in Huppert's front position scaling: $x = Ct^{1/3}$. The front detection process was improved. The Murisic et. al. model [8] using shear-induced migration was shown to characterize the well-mixed state transition to the settled or ridged states with good agreement in power law relations with volume and particle diameters.

The 2015 REU [9] focused on the ridged regime that occurs at higher particle concentrations and incline angles. They found that the most important factor in the height of the ridge was the precursor height on the incline surface. They also investigated the fingering instabilities that often occurred with the ridge regime. Their experimental results suggested that smaller particle size and larger angles of inclination result in a higher quantity of fingers.

This year, during the 2016 REU, we made a major change to the experimental scenario. Instead of constant volume flow, we investigated constant flux flow. Modifications and additions were made to the existing experimental apparatus. These changes led us to significantly rework inherited experimental and measurement methodologies and techniques. The computational image processing and modeling codes were also extensively modified or recreated from scratch. We experimentally varied incline angle and particle concentration; fluid viscosity and particle density were kept constant. Comparisons were made with past constant volume experimental results. In addition to taking the same types of measurements and observations of monodisperse flows as in past years, we made an initial foray into measuring surface velocities. The same general theoretical model from past years was used; however, to account for constant flux, the boundary condition was changed. When compared to the former constant volume scenario, in our experiments the transition from the initial well-mixed state to the final settled or ridged states occurred further down the incline. Also, the fluid/particle front locations moved linearly with t (time) as opposed to $t^{1/3}$.

In section 2 of this report, we work through our theoretical model of particle-laden fluid flow and the numerical methods used to simulate it. In section 3, we describe the experimental equipment, materials, procedures, and the image analysis techniques used to extract measurements from the experiments. In section 4, we first identify limitations of the theoretical model. Then we compare the experimental observations to the model's numerical and qualitative predictions. We end with conclusions and acknowledgements.

2 Theory

2.1 Model

In this section we review the theoretical model in Murisic [8].

We consider a particle-laden thin-film flow of constant flow rate down an incline, as in Figure 1(a). The particles are rigid and negatively buoyant. We assume that the fluid has identical behaviour in y -direction so that the model reduces to be two dimensional, as in Figure 1(b). We further assume that the flow is incompressible and the viscous effect dominates inertial effects (or equivalently, low Reynolds number), so that it can be considered as a Stokes flow.



Figure 1: Setup

The governing equations for our model are then the Stokes equation and the particle transport equation, which read as

$$0 = -\nabla p + \nabla \cdot \underline{\tau} + \rho \underline{g} \quad (1)$$

$$0 = \frac{\partial \phi}{\partial t} + (\underline{u} \cdot \nabla) \phi + \nabla \cdot \underline{J} \quad (2)$$

where p is the fluid pressure, $\underline{g} = (\sin \alpha, -\cos \alpha)^T$, ϕ is the particle volume fraction, $\rho = \phi \rho_p + (1 - \phi) \rho_\ell$ is the density of the fluid, $\underline{\tau} = \mu(\phi)(\nabla \underline{u} + \nabla \underline{u}^T)$ is the stress tensor, and \underline{J} is the particle flux. These equations are accompanied by the incompressibility condition, $\nabla \cdot \underline{u} = 0$. Here the particle flux \underline{J} is due to three factors: gravitational settling, shear-induced migration and viscosity gradient. The functional form for each is established in Acrivos [10], Phillips [11] and Murisic [12]. We have

$$\begin{aligned} \underline{J}_{grav} &= -\frac{d^2(\rho_p - \rho_\ell)\Phi(\phi)}{18\mu_\ell}\phi\underline{g} \\ \underline{J}_{coll} &= -K_c \frac{d^2}{4}(\phi^2 \nabla \dot{\gamma} + \phi \dot{\gamma} \nabla \phi) \\ \underline{J}_{visc} &= -K_v \frac{d^2}{4} \phi^2 \dot{\gamma} \frac{1}{\mu(\phi)} \frac{d\mu}{d\phi} \nabla \phi \end{aligned}$$

Here d is the diameter of particles, $\dot{\gamma}$ is the shear rate, K_c, K_v are experimentally determined constants and $\Phi(\phi) = 1 - \phi$ is the hindrance function. In the above equations, $\mu(\phi)$ is the effective viscosity and it has several different formulas. The one we use for our model is

$$\mu(\phi) = (1 - \frac{\phi}{\phi_m})^{-2},$$

where $\phi_m \approx 0.62$ is the maximum packing fraction. Since the model is two dimensional, we can write $\underline{u} = (u(t, x, z), w(t, x, z))^T$. Then the boundary conditions can be formulated as follows: no-slip at boundaries: $u = w = 0$, at $z = 0$; stress balance on free surface: $(-p\mathbb{I} + \underline{\tau})n = 0$, at $z = h$; kinematic condition: $h_t + uh_x = w$, at $z = h$. Here n is the normal vector on free surface and $h(t, x)$ is the height profile of the flow. The incompressibility of the flow $\nabla \cdot \underline{u} = 0$ translates to $u_x + w_z = 0$.

To further study the above equations, we nondimensionalize them according to the thin-film approximation. This means that the ratio of the height of the flow to the length of the track $\epsilon = H/L \ll 1$. The scales are listed below, as in Murisic [8].

$$\begin{aligned} [x] &= \frac{H}{\epsilon}, \quad [z] = H, \quad [\phi] = 1, \quad [\mu] = \mu_\ell, \quad [u] = \frac{H^2 \rho_\ell g \sin \alpha}{\mu_\ell} = U, \\ [w] &= \epsilon[u], \quad [t] = \frac{[x]}{[u]}, \quad [J_z] = \frac{d^2[u]}{[z]^2}, \quad [J_x] = \epsilon[J_z], \quad [p] = \frac{[u][\mu]}{[z]} \end{aligned}$$

After nondimensionalization of (1) and (2) and imposing boundary conditions, we obtain two decoupled systems of equations, with the first being the equilibrium equations and

the second being the conservation laws.

$$\begin{cases} \phi_z = A(\phi, \sigma) \\ \sigma_z = -\rho(\phi) \end{cases} \quad \begin{cases} h_t + (\int_0^h u \, dz)_x = 0 \\ (h\phi_0)_t + (\int_0^h \phi u \, dz)_x = 0 \end{cases}$$

where

$$A(\phi, \sigma) = \sigma^{-1} \left[1 + \frac{\phi}{\mu(\phi)} \frac{d\mu(\phi)}{d\phi} \frac{K_v - K_c}{K_c} \right]^{-1} \left[-\phi\sigma_z - \frac{2(\rho_p - \rho_\ell)\Phi(\phi)\cot\alpha}{9\rho_\ell K_c} \right]$$

Here $\sigma = \mu(\phi)u_z$ is the stress, $\rho(\phi) = 1 + \phi(\rho_p - \rho_\ell)/\rho_\ell$, and $\phi_0 = \frac{1}{h} \int_0^h \phi \, dz$ is the depth-averaged concentration. The initial condition for the latter system is a piecewise constant function

$$h(0, x) = \begin{cases} h_L, & x < 0 \\ h_R, & x \geq 0 \end{cases},$$

so that the problem is a Riemann problem. The physical meaning of the initial condition is that we have an infinite amount of fluid flowing down the incline with constant height h_L . The initial height h_L is obtained by $\dot{Q} = \rho_\ell g \sin \alpha h_L^3 / (3\mu(\phi))$, where \dot{Q} is the constant flow rate and h_R is the precursor layer height. To further simplify the equations, we apply a change of variable $s = z/h$. The new variables become $\tilde{\phi}(t, x, s) = \phi(t, x, z)$ and $\tilde{u}(t, x, s) = u(t, x, z)/h^2(t, x)$. Then the above systems turn into

$$(3) \begin{cases} \tilde{\phi}_s = A(\tilde{\phi}, \tilde{\sigma}) \\ \tilde{\sigma}_s = -\rho(\tilde{\phi}) \end{cases}$$

$$(4) \begin{cases} h_t + [h^3 f(\phi_0)]_x = 0 \\ (h\phi_0)_t + [h^3 g(\phi_0)]_x = 0, \end{cases}$$

where $f(\phi_0) = \int_0^1 \tilde{u} \, ds$ and $g(\phi_0) = \int_0^1 \tilde{\phi} \tilde{u} \, ds$, together with a boundary condition $\tilde{\sigma}(1) = 0$. If we set $\tilde{\phi}_s = 0$, then we obtain a critical volume fraction, below which the flow is in settled regime and above which the flow is in the ridged regime. The formula for critical volume fraction is found in Murisic [8]:

$$\phi_{crit} = \min \left\{ \phi_m, -\frac{\rho_\ell(B+1)}{2(\rho_p - \rho_\ell)} + \sqrt{\left(\frac{\rho_\ell(B+1)}{2(\rho_p - \rho_\ell)} \right)^2 + \frac{\rho_\ell B}{\rho_p - \rho_\ell}} \right\}$$

where $B = 2(\rho_p - \rho_\ell)\cot\alpha/(9\rho_\ell K_c)$.

2.2 Numerical methods

The numerical method we use to solve system (4) is the finite difference method, or more specifically, the upwind method. The algorithm goes as follows. We need first to find f and g as functions of ϕ_0 . In this case, we fix some $\phi_0 \in [0, \phi_m]$. Then for such a ϕ_0 , we have a system of ODEs (3) together with the boundary condition $\tilde{\sigma}_s(0) = 1$ and the requirement that $\int_0^1 \tilde{\phi} \, ds = \phi_0$, which can be solved numerically for $\tilde{\phi}$ and $\tilde{\sigma}$. By definition of $\tilde{\sigma}$, we can perform an integration to obtain \tilde{u} . From there, we compute the values of f

and g for this specific ϕ_0 : $f(\phi_0) = \int_0^1 \tilde{u} \, ds$ and $g(\phi_0) = \int_0^1 \tilde{\phi} \tilde{u} \, ds$. We repeat the procedure for multiple choices of $\phi_0 \in [0, \phi_m]$ and obtain two sets of data, $\{f(\phi_0^{(1)}), \dots, f(\phi_0^{(N)})\}$ and $\{g(\phi_0^{(1)}), \dots, g(\phi_0^{(N)})\}$. Interpolation is then used to find the functions $f(\phi_0)$ and $g(\phi_0)$. Now with f and g known, we are ready to solve the system (4) by the upwind method, whose formula reads,

$$\underline{U}_j^{k+1} = \underline{U}_j^k - \frac{\Delta t}{\Delta x} (\underline{F}_j^k - \underline{F}_{j-1}^k),$$

where $\underline{U} = (h, h\phi_0)^T$ and $\underline{F} = h^3(f, g)^T$. Here the choices of Δt and Δx are restricted by the CFL condition, where we set $\Delta t = 0.6\Delta x/\lambda$, with $\lambda = \max|3h^2f|$. The initial condition is

$$h(0, x) = \begin{cases} h_L, & x < 0 \\ h_R, & x \geq 0 \end{cases}.$$

3 Experiments and Procedure

We begin this section by describing the equipment and materials used in our experiments. We then describe the preparations and preliminary flow rate measurements needed to conduct the experiments. Finally we detail the camera setup, experimental procedure, and computer programs for front position, height profile, and surface velocity measurements.

3.1 Equipment and Materials

3.1.1 Apparatus

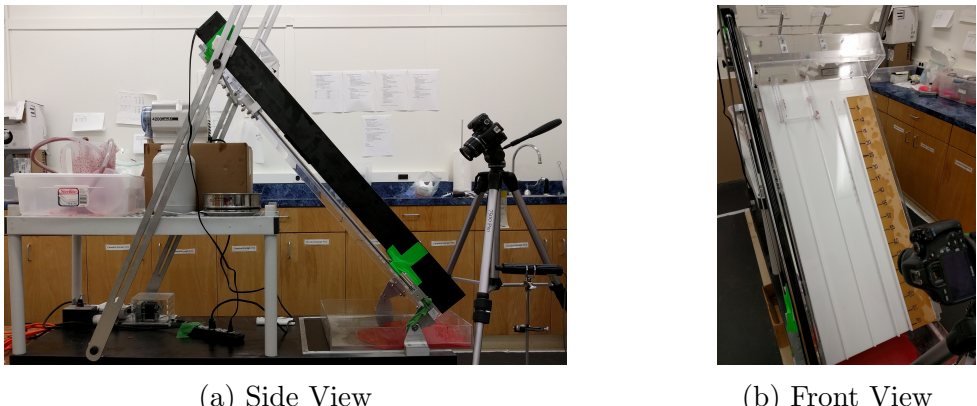


Figure 2: Apparatus

Our apparatus consisted of an inclined acrylic platform with variable angle of inclination α between 12° and 70° . To determine α , we utilized graduated markings along the apparatus as well as a protractor as a secondary check. A level was used to eliminate tilt

in the y-axis direction. The base of our apparatus rested on a lab bench. A collection container rested on the base at the end of the track to capture the fluid after the flow.

Resting on the incline was an opaque acrylic insert with track widths 5 cm and 10 cm, and track heights 1.27 cm and 0.63 cm, respectively. A transparent insert with track width 15 cm and height 1.27 cm was also available, but not used in our trials. Coordinate labels in 5 cm increments rested on the side of the track in the x-direction. Black lights were fixed to the edges of the track for experiments involving fluorescent particles.

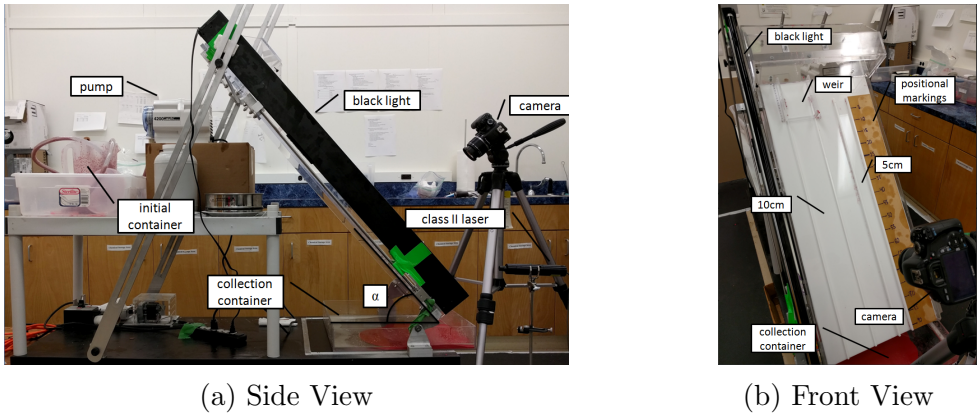


Figure 3: Apparatus

A small piece of acrylic was used as a weir to ensure that the initial profile of the fluid was uniform across the track. The weir fitted perfectly between the walls of the track. Removable acrylic walls were fixed in such a way that prevented the flow of fluid over the track walls.

3.1.2 Pump

A Mityflex 4200 pump was used to provide the constant flow rate in our experiments. The pump is a peristaltic pump for viscous fluids up to 10,000 cSt and could handle particle fluid mixtures. The pump has two controls; one to change the direction of the flow and one to change the flow rate. The first control turns the pump off or switches the motor between clockwise and counter-clockwise, thereby controlling the direction of flow. The second control varies the motor between 2.5% and 100% of the motor's maximum RPM in increments of 2.5%. The flow rate generally increased with motor RPM, but a maximum efficiency was reached at higher RPM due to the high viscosity of the fluid as displayed for pure Polydimethylsiloxane (PDMS) in Fig.6. As viscosity increased, the maximum possible flow rate decreased. At higher volume fractions, the pump reached its maximum efficiency almost immediately, restricting the control we had on flow rate. Fluid left the hose in pulses instead of flowing smoothly due to the nature of peristaltic pumps. This effect was neutralized by using the weir to dam the flow, allowing the steady flow of fluid down the track. Whenever the particle volume fraction changed, the pump had to be purged of particles by pumping pure PDMS through the hose until all of the particles were removed.

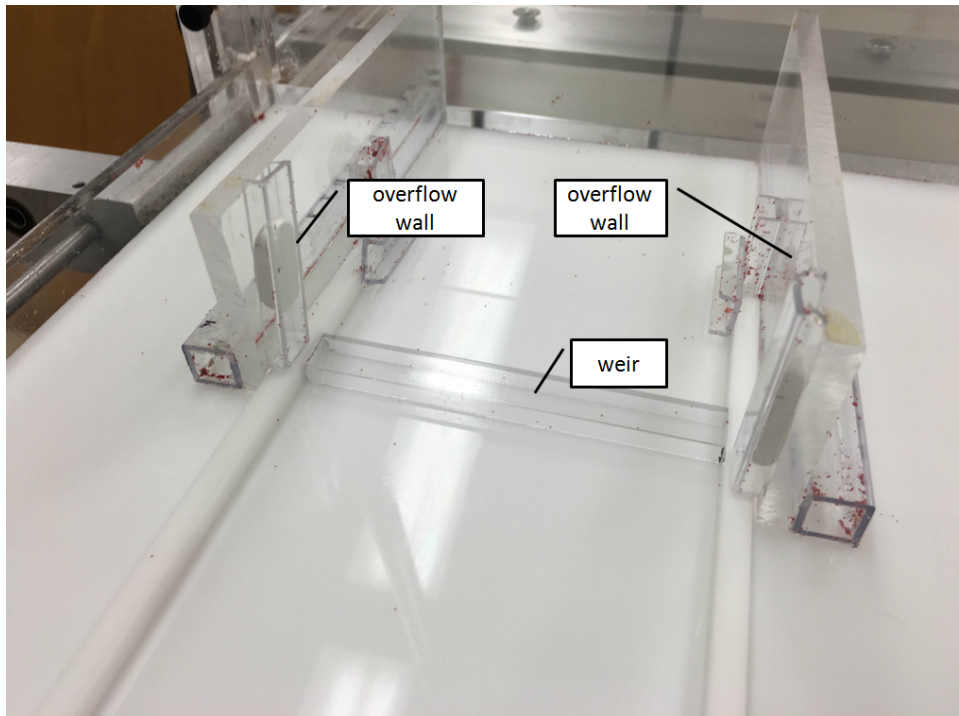


Figure 4: Weir

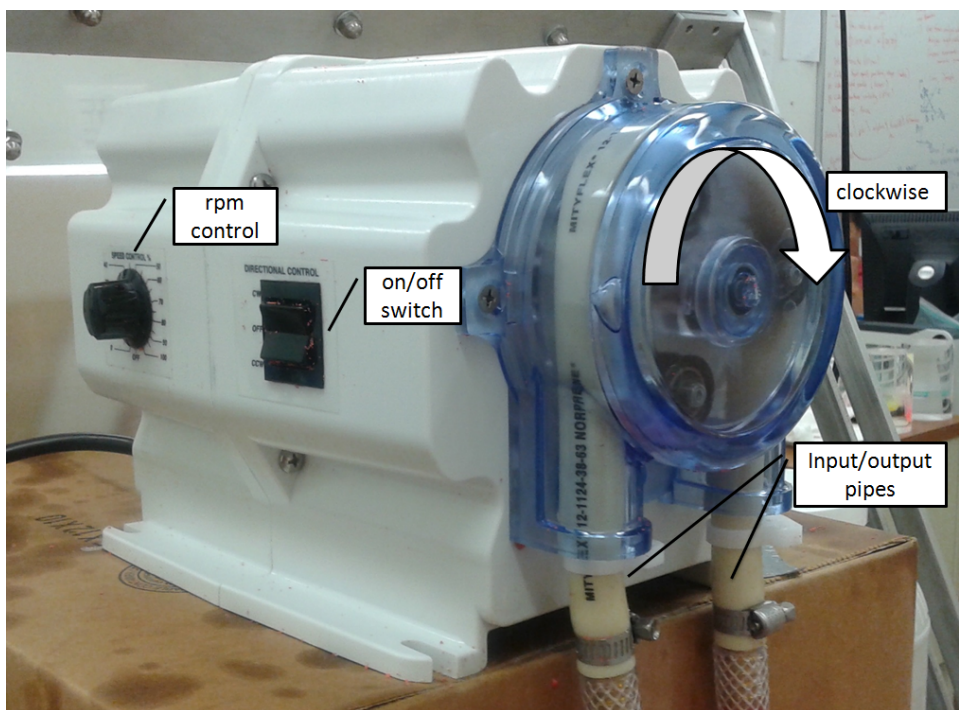


Figure 5: Pump

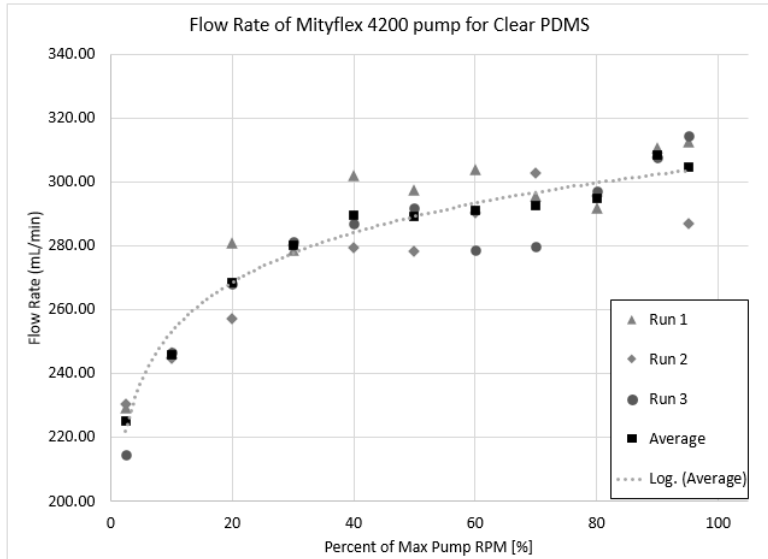


Figure 6: Pump Flow Rate in mL/min vs Percent of max RPM. The trendline is a logarithmic fit to the data for the average of each trial.

3.1.3 Laser

A green Class II line laser was used to obtain height profiles in our experiments. To use the laser effectively, all other sources of light were turned off during the trials.

3.1.4 Camera

We used a Canon EOS Rebel T2i camera to collect data. The camera was equipped with a program called Magic Lantern¹ to allow pictures to be taken in intervals. The camera settings will be described under each experimental procedure. An expandable tripod was used to fix the camera in its desired position.

3.1.5 Materials

To suspend our particles, we used Polydimethylsiloxane (PDMS). PDMS has a density $\rho_\ell = 9.71 \text{ g/cm}^3$. Our experiments used PDMS with a kinematic viscosity of 1000 cSt because it allowed us to adjust the particle volume fraction and stay within the pump's specifications.

We used GSB-3 particles for preliminary study and DB-4501-187-LS Red-Deco Beads for our actual experiments. The Deco Beads were already colored and therefore easy to detect on a video. The GSB-3 particles have diameter and density 0.595-0.841 mm and $\rho_p = 2.475 \text{ g/cm}^3$ respectively while the Deco Beads have diameter and density 0.25-0.50 mm and $\rho_p = 2.5 \text{ g/cm}^3$ respectively.

¹<http://www.magiclantern.fm/>

Cospheric Fluorescent yellow-green polyethylene microspheres with diameter 300-355 μm were used to track the surface velocity. These tracer particles glow brightly under black lights and allowed us to easily isolate their position over time in a video.

3.2 Dyeing Procedure

To dye particles, we mixed them up in a jar with a small amount of acrylic paint and toasted them on 250° for 20 minutes until they formed a nice crust. Then we removed the freshly baked particles and left them out to cool. Once the particles cooled to a safe level, we transferred them to a plastic bag. We then pounded the particles until the particles were no longer clumped.

To dye the fluid for front position measurements, we mixed a small amount of Py-lakrome powder in the PDMS until the color was uniform.

3.3 Preparation of Particle Slurry

To prepare a mixture with a specific particle volume fraction, we first added an appropriate amount of PDMS to a container and measured the mass of the PDMS with a scale. Each experiment consumed about 0.5 L of PDMS. Then we calculated the mass of particles needed for our particle volume fraction with the formula

$$\frac{\phi}{1 - \phi} \frac{m_\ell}{\rho_\ell} \rho_p = m_p.$$

3.4 Flow Rate Measurements

All experiments were carried out with the flow rate at 2.5% of the maximum RPM. However, as particle volume fraction, and therefore viscosity, changed, the flow rate changed as well. Therefore flowrate measurements were taken before each experiment.

The mass of the particle mixture pumped into a container was measured over a time interval. This was done five times. We continuously stirred the particle mixture so we could assume the mixture was homogeneous. We calculated the volume pumped using the density of the mixture

$$\rho_{mix} = \phi \rho_p + (1 - \phi) \rho_\ell.$$

Finally we averaged the flow rates to find our accepted value as summarized in Table 1.

3.5 Front Position Experiments

Experiments were carried out to measure the position of both the particle and fluid front. In the well mixed and ridged regimes, these fronts are identical but in the settled regime the fluid separates from the particles. Therefore the PDMS had to be dyed in front position experiments to provide enough contrast for image analysis.

Trial	Flow rate (mL/s)		
	Deco Beads $\phi = 0.25$	GSB-3 $\phi = 0.3$	Deco Beads $\phi = 0.4$
1	1.91	1.96	1.09
2	2.01	1.81	1.12
3	2.86	1.77	1.13
4	1.88	1.75	1.14
5	1.89	1.62	1.13
Average	1.91	1.78	1.12
Range	0.15	0.34	0.05

Table 1: Flow Rates for Deco Beads ($d = 0.25\text{-}0.50 \text{ mm}$) and GSB-3 ($d = 0.595\text{-}0.841 \text{ mm}$). All flow rates were conducted at 2.5% of max RPM. Particle volume fractions tested were $\phi = 0.25, 0.3, 0.4$

3.5.1 Camera Setup

To capture the front position for MatLab analysis, the camera was positioned at the base of the track at a 90° angle relative to the track. The camera recorded a video of the fluid moving down the track with the movie exposure set to auto. The room lights remained on throughout this experiment.

3.5.2 Procedure

The particle slurry was pumped from its container onto the incline next to the track to purge any settled mixture. The mixture was stirred in its container to ensure a uniform consistency. The camera began recording and the hose was moved to the track behind the weir. We stirred the mixture behind the weir by moving a stir stick back and forth along the upstream edge of the weir to keep the mixture from settling and to approximate a uniform flow. The mixture was allowed to run the length of the track. Once the mixture reached the end of the track, the video was stopped and the experiment was concluded.

The video for front position was then converted to a sequence of frames using the Matlab script 'mov2imcolor.m.' Each individual frame was cropped and pieced back together using 'photocropper.m' then 'photocropperwidth.m' such that the track and measurement lines were adjacent with all extraneous information removed. Two different scripts were used to process the different regimes. For the well mixed and ridged regimes, 'monodisperse_processor.m' was used to determine front position and velocity. This was done by taking a frame and selecting enough points to create a suitable threshold that would be able to track the front. For the settled regime, 'settled_monodisperse_processor.m' was used where thresholds for both the fluid and particle front were needed. Samples of the front tracking are shown in Figure 7

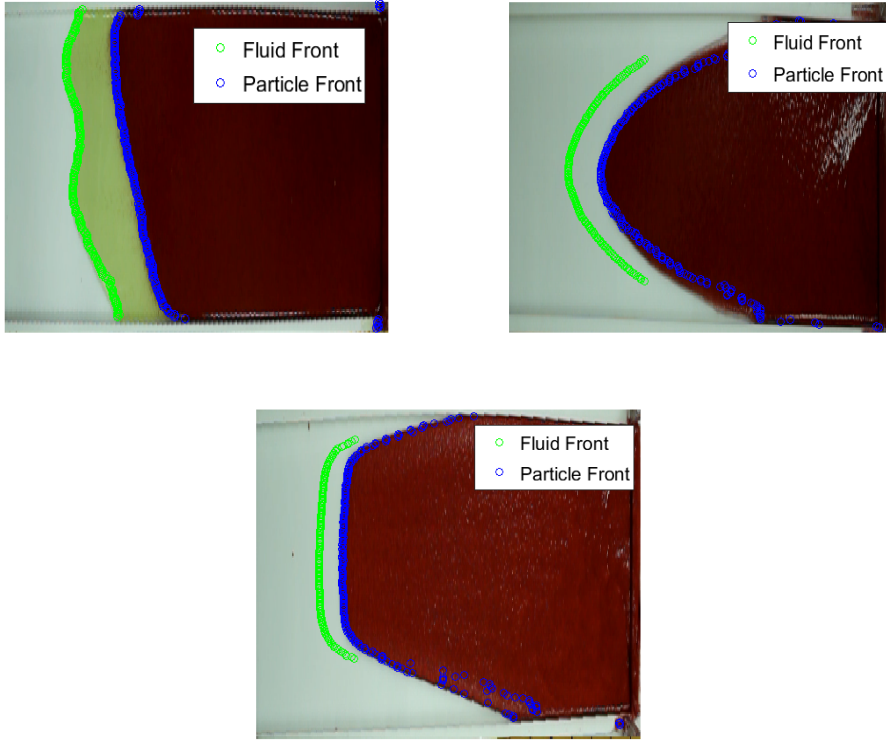


Figure 7: Example of processed frames with the front tracking overlaid on top. The green edge represents the fluid front, while the blue edge represents the particle front. The top left image shows the settled regime. The top right image shows the well mixed regime. The bottom image shows the ridged regime.

3.6 Height Profile Experiments

The height profile data was collected with a video of the laser line on the thin film. We were particularly interested in the x-direction height profile so the laser was oriented along the length of the track. The height was calculated in MatLab by using the displacement of the laser line relative to a reference image.

3.6.1 Camera Setup

The camera was placed to the side of the apparatus and tilted to same angle as the incline. The camera was then angled 45° relative to the track. A video was taken for height profile with the ISO set to 1600 and the aperture set to 6.4 at 30 frames per second. The focus was manually set with the lights on. Note that these camera settings are subject to change depending on environment, laser intensity, and desired exposure.

3.6.2 Procedure

The laser was oriented in the x-axis direction. All sources of light besides the laser were eliminated. A reference image was taken of the laser line on a clean track, and a calibration image was taken of the laser line across an object whose height is known. Images of the laser line as the flow moved down the track were later processed in MATLAB.

The video recording began and the fluid was pumped down the track in a similar manner to the front position experiments. The well mixed and ridged regimes could be accurately captured but the settled regime could not due to the laser passing through the clear fluid.

A dusting technique was discussed to improve the quality of data collected. Dusting the fluid with Z-Light Spheres G-3125 prevents the laser from penetrating the clear PDMS. However, we discovered that dusting at the front significantly changes the flow.

The video collected during our experiments with the laser line was converted to a sequence of frames with a MATLAB script 'mov2imBW.m.m'. The frames were then processed with the script 'lengthheightmain.m'. In this script, height profile was measured by the displacement of the laser line by the slurry from the laser line in the reference frame. First the calibration image was analysed to derive the ratio of pixels to mm in the image. Then the data image was processed. A smoothing function was applied to reduce the noise. The resulting height profile was then compared to the predicted height from the numerical solution to our model.

3.7 Surface Velocity Experiments

To take surface velocity, we tracked fluorescent tracer particles as they floated along the fluid. The low concentration and neutral buoyancy of the tracer particles allowed us to assume that they probably did not impact the flow behavior. The resulting data was analyzed using a Particle Tracking Velocimetry (PTV) program in MATLAB.

3.7.1 Camera Setup

The camera was positioned in front of the incline, perpendicular to the slope. The center of the camera frame was positioned as close to the middle of the track as the tripod would allow. The video used the following settings: ISO 6400, aperture f8.0, 30 fps. The camera was manually focused in the light. Note that these settings may change depending on the desired exposure.

3.7.2 Procedure

First we measured the range of the track that the camera captures. Then we measured the distance of the camera lens from the surface of the track. The black lights were turned on and all other light sources were eliminated. The camera then began recording. The fluid was pumped behind the weir similar to the method used for front position and height profile experiments. As the flow moved down the track, tracer particles were sprinkled onto the film. The concentration of the particles is of vital importance to

the accuracy of the PTV program. The concentration had to be very sparse and yet be present throughout the range of the track. Clumping of the tracer particles led to inaccurate results in the PTV program. Once the fluid reached the end of the track, the experiment was concluded.

The video collected during our experiments with fluorescent tracer particles was converted to a sequence of frames with a MATLAB script 'mov2imBW.m.m'. The resulting frames were processed by the script 'PTVmain.m'. In this script, a bandpass filter is applied with a specified threshold to filter out image noise and improve contrast. Particles are seen in each image as bright Gaussian blobs on a dark background. Searching for brightness maxima yields approximate pixel location for the particles, which are then refined to subpixel accuracy.

After particles are identified in two consecutive frames, every possible matching is considered. The parameter D is the maximum possible displacement of a particle between any two frames. The total displacement of a matching is computed. Any matching that requires a particle to move more than D is penalized by increasing the total displacement by a factor of D^2 . The matching that corresponds to the minimum total displacement is taken as the correct matching. Applying this to several frames yields the position of a particle in time, from which we determined velocity. The main routines to track particles were obtained from an open-source repository. [13].

4 Results

4.1 Comparing Model Predictions with Observations

We begin with some observations of the limitations of the current theoretical model. Though in theory the model predicts the position of the fronts in time well, the model rests on the key assumption that the fluid has equilibrated in the z-direction. Observation during experiments with the pump leads our team to believe that this equilibration takes a significantly greater distance to occur in the constant flow case than the constant volume case. Since we lacked the means to determine when exactly our slurries achieved this state, we can only observe the behavior of the slurry from the top of the track, rather than from when the model assumptions first become valid. As a result, theoretically predicted velocities and positions in time tended to differ by a wide margin from our experimental results. In addition, the model currently ignores wall effects, which are clearly present and non-trivial in experiments. For example, in experiments at low angles we observed fingers in the slurry forming along the walls, possibly as a result of the walls exerting an attractive force on the fluid. It is entirely possible that these wall effects have a significant impact on the behavior of the experiments on the whole. Up to this point we have lacked sufficient quantitative data to properly tune our theoretical model. For this reason a major focus of the 2016 REU was developing PTV as an accurate source of quantitative data. The next few sections will discuss the analysis techniques we found to be the most useful for creating results that could be directly compared with model predictions.

4.2 Front Position

Using the front position tracking mentioned previously, we were able to plot front position with respect to time (Fig. 8). The relationship between calculated front position and time was clearly seen to be linear. This relationship qualitatively validates the theoretical model; however, the values for front velocity observed did not match the solutions obtained from numerical simulations. The observed front velocities were .60 cm/sec ($\phi = 0.25$ and $\alpha = 20^\circ$), 1.5 cm/sec ($\phi = 0.25$ and $\alpha = 50^\circ$), .85 cm/sec ($\phi = 0.40$ and $\alpha = 50^\circ$) for the settled, well mixed, and ridged regime respectively. The numerical simulations predict that the front speeds should be .35 cm/sec, .68 cm/sec, and .93 cm/sec for the respective regimes. While the experimental are on the same scale as the predicted values, this marked difference signals that more observations must be done.

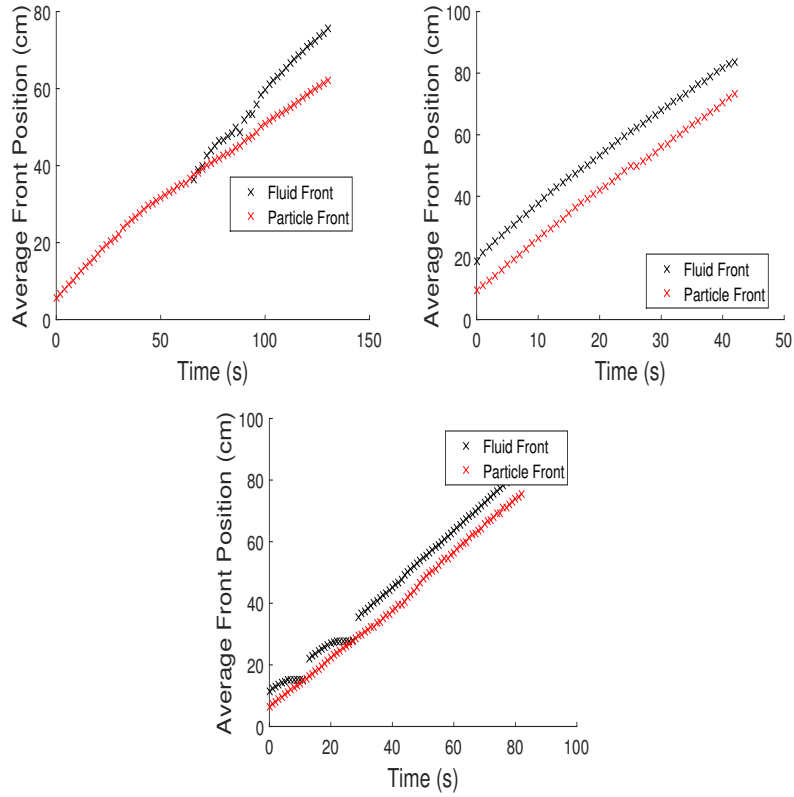


Figure 8: Graphs of average front position versus time for the three different regimes. The top left plot shows the settled regime with $\phi = 0.25$ and $\alpha = 20^\circ$. The top right plot shows the well mixed regime with $\phi = 0.25$ and $\alpha = 50^\circ$. The front positions in the well mixed case seem to indicate that the fronts are separated; however this is not the case. This was just an example of an error in front tracking. The bottom plot shows the settled regime with $\phi = 0.40$ and $\alpha = 50^\circ$.

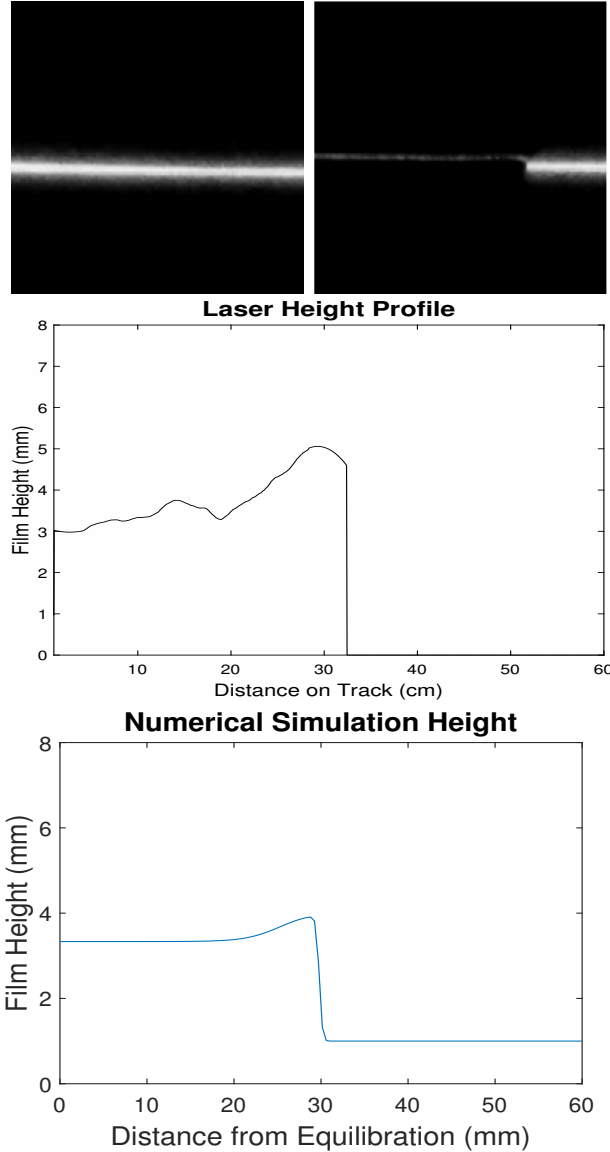


Figure 9: Example of data obtained from laser measurements. On the top left is the reference image, and the top right shows the reference line being displaced by fluid flowing from the left. In the middle is the height profile according to laser measurement. At the bottom is the numerical simulation of the height profile. These were taken from an experiment with $\phi = 0.4$ and $\alpha = 50^\circ$, where we expect to see the ridged regime. Note the numerical simulation plots the height of the precursor layer as well as the height of the slurry.

4.3 Height Profile

Comparison of the measured height profile with the numerical simulations worked better than some of our other quantitative measurements because once a final state is achieved the change in film height over time is relatively slow. Our model predicted an

average fluid height of 3.3 mm rising to a ridge with average height of 3.8 mm. Our experimental measurements agreed well with values of 3.1 mm and 4.2 mm, respectively. (Fig. 9) The differences between measurements and numerical simulations were within measurement error, which we determined to be approximately 0.5 mm by measuring the height of a ruler of uniform known height.

4.4 Surface Velocity

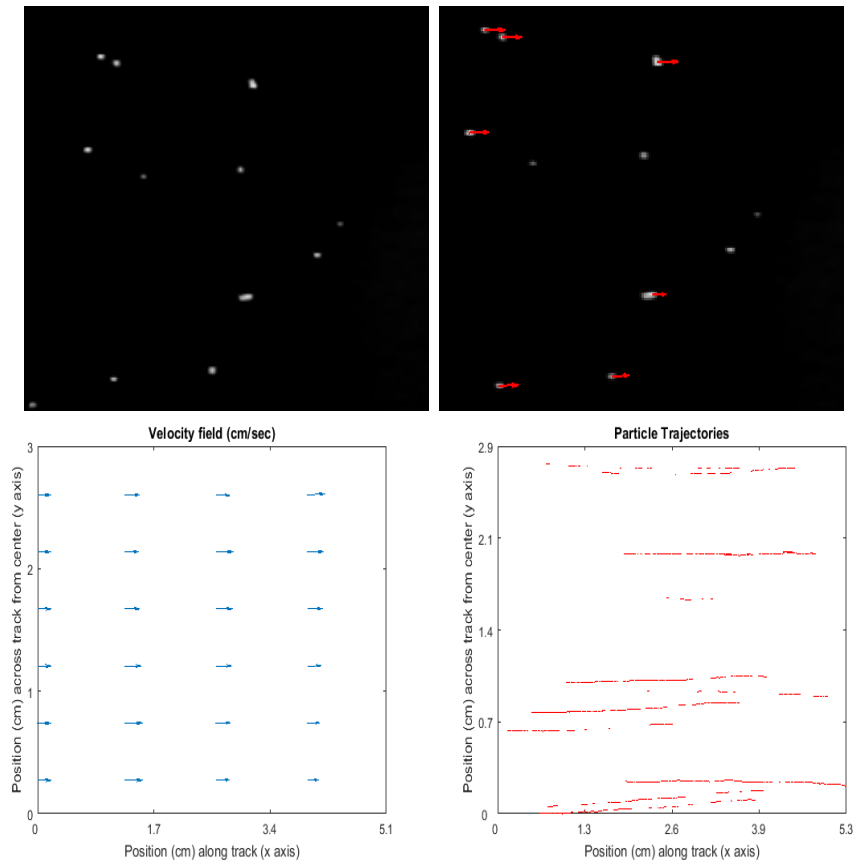


Figure 10: Top left: sample data image, top right: example of the tracked particle trajectories, bottom right: velocity field extrapolated from the particle trajectories, bottom right: particle trajectories through time. Data taken from an experiment with $\phi = 0.25$ and $\alpha = 20^\circ$.

Refining our PTV experimental procedure took a good portion of the summer. As a result, we did not have time to capture PTV data of sufficient quality for all of our experimental parameters. However, the following analysis we performed on the experiment at $\phi = 0.25$ and $\alpha = 20^\circ$ (Fig. 10) shows that this new quantitative data is both useful and agrees with the model.

A few results are immediately clear. The first is that the model assumption that in the slurry the y-component of the velocity is zero is well founded. Particles were observed

to move down the slope parallel to the track. In the center of the slurry immediately behind the front the measured surface velocity was 0.74 cm/sec down the track. By way of comparison, the measured particle front speed was 0.40 cm/sec and the fluid front had a speed of 0.60 cm/sec. This agreed with qualitative observations made during the experiment. The model predictions and the experimental observations disagreed even on the qualitative level. The model predicted a surface velocity of 0.35 cm/sec, which is slower than even the particle front speed. That prediction was completely contradicted by experimental observation, as we could see surface tracer particles flowing over the slurry and catching up to the fluid front. This predictive failure is likely due to the limitations of the model mentioned at the beginning of this section, and the fact that the model currently has no y -dependence. Since surface velocity theoretically has a parabolic profile in y , the similarity between the measured and predicted surface velocity would depend in large part on where in the slurry one chose to take the measurement. However, since the predicted surface velocity is very clearly erroneous even in that case, either the numerical simulation has errors that must be corrected, or there is a need to further refine the theoretical model to improve predictive accuracy.

5 Conclusion

Given how well the current model has performed in the past in the constant volume case, in this project we sought to propel the research here into the next phase, examining constant flow particle slurries. In order to confirm the continued validity of the model in these new conditions, we adapted and refined past experimental techniques to collect quality quantitative data with our new experimental apparatus. In addition, revisions of past analysis techniques were developed that more accurately processed the measurements gathered. Through these new methods we were able to qualitatively confirm the current model for constant flow rate. These qualitative observations included accurately predicting the different regimes and the linear relationship of front position with time. However, varying degrees of disparity were observed in all three measurements when comparing the quantitative experimental data with numerical simulations of the current theoretical model. Further investigation is needed to determine the source of these disparities, as they may result either from simplifications made in the model, neglected factors such as wall effects, or simply errors in the numerical simulations. This research has matured to the point that a large volume of accurate quantitative data will be of great use. It is our hope that we have laid the groundwork to make gathering that data possible.

Acknowledgements

The 2016 UCLA particle slurry team would like to thank the REU director, Professor Andrea Bertozzi and the team's mentors, Dr. Michael Lindstrom and Jeffrey Wong, for all their advice and support. Aviva Prins would like to thank the Science Research Initiative's Summer Scholars Research Program for funding.

References

- [1] Wylie Rosenthal, Spencer Hill, Paul Latterman, and Paul David. *Gravity Driven Flow of Particle-Laden Thin Films*, 2011 (accessed August 5, 2016). Available online at http://www.math.ucla.edu/~bertozzi/WORKFORCE/Summer2011/Slurry-Flow-2011/Final_Report_Slurry_Flows.pdf.
- [2] Herbert E Huppert. Flow and instability of a viscous current down a slope. *Nature*, 300(5891):427–429, 1982.
- [3] Benjamin P Cook, Andrea L Bertozzi, and AE Hosoi. Shock solutions for particle-laden thin films. *SIAM Journal on Applied Mathematics*, 68(3):760–783, 2008.
- [4] Thomas Ward, Chi Wey, Robert Glidden, AE Hosoi, and AL Bertozzi. Experimental study of gravitation effects in the flow of a particle-laden thin film on an inclined plane. *Physics of Fluids (1994-present)*, 21(8):083305, 2009.
- [5] Kali Allison, Thomas Crawford, Saro Meguerdijian, Wylie Rosenthal, and Gilberto Urdaneta. *Particle-Laden Flows: Final Report*, 2012 (accessed August 5, 2016). Available online at <http://www.math.ucla.edu/~bertozzi/WORKFORCE/Summer2012/REU%202012/Particle%20Slurries/Final.pdf>.
- [6] Matt Hin, Kaiwen Huang, Shreyas Kumar, and Gilberto Urdaneta. *Particle Laden Flows*, 2013 (accessed August 5, 2016). Available online at <http://www.math.ucla.edu/~bertozzi/WORKFORCE/REU%202013/Particle%20Flow/Report.pdf>.
- [7] Sarah Burnett, Andrew Li, Matthew Molinare, and Katherine Varela. *Gravity driven particle-laden flow*, 2014. Available internally.
- [8] Nebojsa Murisic, Benoit Pausader, Dirk Peschka, and Andrea L Bertozzi. Dynamics of particle settling and resuspension in viscous liquid films. *Journal of Fluid Mechanics*, 717:203–231, 2013.
- [9] Sarah Burnett, Jesse Kreger, Hanna Kristensen, and Andrew Stocker. *Dynamics of particle-laden thin films: viscous fluid on an incline*, 2015. Available internally.
- [10] David Leighton and Andreas Acrivos. The shear-induced migration of particles in concentrated suspensions. *Journal of Fluid Mechanics*, 181:415–439, 1987.
- [11] Ronald J Phillips, Robert C Armstrong, Robert A Brown, Alan L Graham, and James R Abbott. A constitutive equation for concentrated suspensions that accounts for shear-induced particle migration. *Physics of Fluids A: Fluid Dynamics (1989-1993)*, 4(1):30–40, 1992.
- [12] N Murisic, J Ho, V Hu, P Latterman, T Koch, K Lin, M Mata, and AL Bertozzi. Particle-laden viscous thin-film flows on an incline: Experiments compared with a theory based on shear-induced migration and particle settling. *Physica D: Nonlinear phenomena*, 240(20):1661–1673, 2011.

- [13] D Blair and E Dufresne. The matlab particle tracking code repository. Accessed July 11, 2016.